RSC Advances

RSC Publishing

PAPER

View Article Online
View Journal | View Issue

Self-assembled graphene@PANI nanoworm composites with enhanced supercapacitor performance†

Cite this: *RSC Advances*, 2013, **3**, 5851

Yongsong Luo,‡[abd] Dezhi Kong,‡[ab] Yonglei Jia,[b] Jingshan Luo,[a] Yang Lu,[b] Deyang Zhang,[b] Kangwen Qiu,[b] Chang Ming Li[c] and Ting Yu*[ade]

Received 22nd October 2012,
Accepted 8th February 2013

DOI: 10.1039/c3ra00151b

www.rsc.org/advances

Self-assembled hierarchical graphene@polyaniline (PANI) nanoworm composites have been fabricated using graphene oxide (GO) and aniline as the starting materials. The worm-like PANI nanostructures were successfully obtained *via* a simple polymerization route. The graphene-wrapped hierarchical PANI nanoworm structures could be prepared using a three-step process by dispersing the PANI nanoworms sequentially into the relevant solution. The morphologies and microstructures of the samples were examined by X-ray diffraction (XRD), scanning electron microscopy (SEM), transmission electron microscopy (TEM), X-ray photoelectron spectroscopy (XPS) and Raman spectroscopy. Electrochemical properties were also characterized by cyclic voltammetry (CV) and galvanostatic charge–discharge. The results indicated that the integration of graphene and the worm-like PANI nanocomposites possessed excellent electrochemical properties. These hierarchical worm-like graphene@PANI nanostructures could afford an interconnected network with a lot of well-defined nanopores, and further provided more active sites and excellent electron transfer path for improving the electric conductivity as well as good mechanical properties. Supercapacitor devices based on these self-assembled nanocomposites showed high electrochemical capacitance (488.2 F g^{-1}) at a discharge rate of 0.5 A g^{-1}, which also could effectively improve electrochemical stability and rate performances.

1 Introduction

In the wake of the fast depleting traditional energy resources and the rising environmental protection concepts, the development of renewable energy production, growing demand for portable systems and hybrid electric vehicles have been attracting much attention.[1] Extensive efforts have gone into developing lithium ion and other advanced rechargeable batteries to store energy for autonomy purposes.[2] Compared with rechargeable batteries, electrochemical capacitors, also known as supercapacitors, can display large power density, moderate energy density, good operational safety, and long cycling life and hence are highly desirable as a modern energy storage system.[3] Therefore, to enable supercapacitor devices for broad applications, a range of nanoscale building blocks as electrode materials have been investigated extensively.[4–6] In particular, a great deal of research on electrochemical capacitors has also focused on increasing both power and energy density as well as lowering fabrication costs while using environmentally friendly materials.[7] Currently, high surface carbon and transition metal oxides are the main families of electrode materials being investigated for supercapacitor applications.[8] Some high surface carbon materials, such as carbon nanotubes (CNTs), have long cycle life and good mechanical properties, but unsatisfactory specific capacitance.[9] Some of the transition metal oxides, such as RuO_2, exhibit remarkably high specific capacitance and excellent reversibility.[10] However, the high cost and toxicity to the environment have greatly limited its practical application. Therefore, designing a supercapacitor device with appropriate performance characteristics remains a significant challenge even today.

Graphene, a two-dimensional monolayer of sp^2-bonded carbon atoms with unique electronic and mechanical properties, has received a rapidly growing research interest.[11–15] Graphene has attracted considerable attention in the areas of fabricating electronic and energy storage devices, sensors, transparent electrodes, electromagnetic shielding devices, high strength composite materials and anticorrosion coat-

[a]*Division of Physics and Applied Physics, School of Physical and Mathematical Sciences, Nanyang Technological University, 637371, Singapore. E-mail: yuting@ntu.edu.sg*
[b]*Department of Physics & Electronic Engineering, Xinyang Normal University, Xinyang 464000, P. R.China*
[c]*Institute for Clean Energy and Advanced Materials, Southwest University, Chongqing 400700, P. R China*
[d]*Energy Research Institute at Nanyang Technological University (ERIAN), 639789 Singapore*
[e]*Department of Physics, Faculty of Science, National University of Singapore, 117542 Singapore*

† Electronic supplementary information (ESI) available. See DOI: 10.1039/c3ra00151b

‡ These authors contributed equally to this work

ings.[16–18] In addition, graphene-based materials can be easily obtained by simple chemical processing of graphite.[19] Therefore, the potential of using graphene-based materials for supercapacitor has attracted much attention in recent years.[20,21] In particular, nanocomposites containing graphene and conducting polymer components such as polyaniline (PANI), polypyrrole (PPY), polythiophene (PTH), polyphenylene (PPH) and their derivatives have been extensively investigated for the supercapacitor electrode.[22–25] Among these materials, PANI has been considered as one of the most promising electrode materials because of its low cost, easy synthesis and relatively high conductivity and environmental stability.[26,27] For example, Shi *et al.*[28] obtained composite films of chemically converted graphene and PANI nanofibers by vacuum filtration of the mixed dispersions of both components. Zhang *et al.*[12] synthesized similar composites by *in situ* polymerization of aniline monomer in the presence of graphene oxide under acidic conditions. Wang *et al.*[29] used a three-step *in situ* polymerization reduction/dedoping–redoping process. However, the observed capacitance values are mainly limited by the agglomeration of graphene sheets and do not reflect the intrinsic capacitance of an individual graphene sheet. Therefore, developing large surface area, good dispersion degree, and combining materials with excellent conductive activity are the crucial factors to address this issue for supercapacitors.

In this work, a novel hierarchical graphene@PANI nanoworms composite was successfully synthesized, serving as an electrode material for supercapacitors. First, the special worm-like structure materials would create some channels for the effective transport of electrolyte owing to the intensive thorn-like convex structure on the surface of PANI. Meanwhile, it is useful for reducing device resistance and nanoporosity with large surface area to allow faster reaction kinetics. Second, the capacitance has been dominated by the pseudocapacitance from graphene sheets wrapped on the PANI nanoworms surface, and the electric double layer capacitance from the graphene sheet has been enough utilized due to the monodispersion of individual graphene sheets on the surface of the polymer matrix. Third, all PANI nanoworms consist of an ultrathin surface layer, which is capable of contributing to interfacial electrochemical reactions by providing a large electrode surface area. Moreover, graphene is a good electron acceptor, and PANI is a good electron donor. The graphene could not only offer a good conducting pathway, but also an excellent wrapping material for enduring large volume changes as well as displaying good strain accommodation. Undoubtedly, these can contribute to improving the capacity and cycle life of supercapacitors.

2 Experimental section

2.1 Synthesis of the PANI nanoworms

All reagents used were of analytical grade and were used directly without any purification. In a typical synthesis procedure,[30] the purified aniline (20 mL, 0.22 mol) was dissolved in HCl aqueous solution (22.5 mL HCl added to 100 mL of H_2O). The mixture was stirred for 30 min in an ice bath. Then $(NH_4)_2S_2O_8$ (APS, 26 g, 0.11 mol) dissolved in 50 mL of DI water was slowly (about 60 mL h^{-1}) added into the acid aniline solution. The mixture was allowed to stir at room temperature for 12 h, polymerization was completed, and the suspension was dark green. The precipitated polymer was collected by filtration and repeatedly washed with DI water until the filtrate became neutral. At this point, the acid doped product of PANI was obtained. The remaining product of the above filtration was added into 100 mL of concentrated ammonia. After stirring for about 24 h, the precipitated polymer was collected by filtration and repetitively washed with DI water until the filtrate became neutral, and finally dried under vacuum at 60 °C to obtain the product as a deep blue powder.

2.2 Synthesis of graphene@PANI nanoworm composites

Graphene oxide (GO) was prepared using a modified Hummers method.[31] To fabricate graphene-wrapped PANI nanoworms, a general strategy could be achieved by dispersing the PANI nanoworms sequentially into the following three solutions for varied durations at room temperature.[32] Typically, some fresh PANI nanoworm powders (10 mg) were first added into 1 g L^{-1} poly(allylamine hydrochloride) (PAH) solution and then dispersed by ultrasonication for 1 h. Next, the above reaction solution was dispersed into 0.2 g L^{-1} GO solution with the aid of ultrasonication and vigorous stirring at 0 °C for 5 h. Subsequently, 20 μL of hydrazine solution (N_2H_4, 80 wt% in water) was added, and the mixture solution was heated at 98 °C for 1 h. Finally, the sample was collected by filtration, washed with deionized water, and dried at 60 °C to obtain the graphene@PANI nanoworm composites.

2.3 Characterization

The phase purity of the products was characterized by X-ray powder diffraction (XRD) using a D8 Focus (Germany, Bruker) automated X-ray diffractometer system with Cu-Kα radiation (λ = 1.5418 Å). Scanning electron microscopy (SEM) images were obtained using a HITACHI S-4300 microscope (Japan). Transmission electron microscopy (TEM) observations were carried out on a JEOL JEM-2010 instrument in bright field and on a HRTEM JEM-2010FEF instrument (operated at 200 kV). The surface area was measured using a Micromeritics (NOVA 4200e) analyzer. The nitrogen adsorption and desorption isotherms were obtained at 77.35 K. The Brunauer–Emmett–Teller (BET) surface area was calculated from the linear part of the BET plot. Raman spectra were record using a micro-Raman spectrometer (Witech CRM200, the excitation wavelength at 532 nm). X-ray photoelectron spectroscopy (XPS) spectra were measured on a PerkinElmer model PHI 5600 XPS system with a resolution of 0.3–0.5 eV from a monchromated aluminum anode X-ray source. The impedance spectra were recorded upon the application of the bias potentials in the frequency range 10 mHz to 10 kHz, using an AC voltage of 5 mV amplitude.

2.4 Electrochemical measurements

The working electrode was prepared by the solvent evaporation method, an appropriate amount of the graphene@PANI nanoworm (or pure PANI nanoworm) powders and a little amount of acetylene black (mass ratio about 9 : 1) were dispersed in 5 mL *N*-methyl pyrrole (NMP) by ultrasonication for 10 min. The titanium substrate was polished with emery paper, then rinsed thoroughly with ethanol and distilled water, and finally dried by blower. The graphene@PANI nanoworm (or pure PANI nanoworm) suspension was dripped onto the titanium substrate. The electrode was dried under an infrared lamp before the electrochemical test. A three-electrode cell system was used to evaluate the electrochemical performance by electrochemical impedance spectroscopy (EIS), cyclic voltammetry (CV), and galvanostatic charge–discharge techniques on an electrochemical workstation (CHI 760C, CH Instruments Inc., Shanghai) at room temperature. All electrochemical experiments were carried out in 1 M H_2SO_4 aqueous solution, the three electrode cell configuration consisted of Pt as the counter electrode, Ag/AgCl as the reference electrode, and the titanium substrate of coated samples as the working electrode. The CV curves were collected with a potential range from −0.1 to 0.9 V *versus* reference electrode at various scan rates ranging from 10 to 200 mV s^{-1}. The EIS measurements were performed over a frequency range from 0.01 Hz to 100 kHz by applying an alternate current (AC) signal of 5 mV in amplitude throughout the tests under an open circuit state. Galvanostatic charge–discharge measurements were run from −0.1 to 0.9 V at a current density of 0.4 to 3 A g^{-1}, and open circuit potential. The specific capacitances were calculated according to $C = (I\Delta t)/(\Delta V \times m)$, where I is the constant discharge current, Δt is the discharge time, ΔV is the voltage drop upon discharging (excluding the IR drop), m is the total active substance mass of the electrode material.[33]

3 Results and discussion

The XRD patterns of graphite, GO, graphene, pure PANI and graphene@PANI nanoworm composites are shown in Fig. 1. The natural graphite exhibits a higher intensity with the diffraction peak at $2\theta \approx 26.3^\circ$, indicated that the spatial arrangement of the pure graphite microchip layer is very neat, and it is also correlated to an interlayer spacing of about 0.34 nm by the Prague formula calculation at the (002) diffraction peak. In the XRD pattern of the GO, the (002) layer spacing of the diffraction peaks left shift to $2\theta \approx 10.6^\circ$, and its intensity decreased relatively, which is attributed to (001) reflections. After reduction into pure graphene, this peak nearly disappears, but another broad reflection peak centered at $2\theta \approx 23^\circ$ was observed in the XRD pattern of graphene, which can be correlated to an interlayer spacing of single or a few layers in the graphene sample. The observed broad peak also indicates that the graphene sheets are loosely stacked, and it is different from the crystalline graphite.[12] The pure PANI sample exhibits a broad reflection peak at around $2\theta \approx 23.6^\circ$, which is characteristic of the polymer. In addition, another broad reflection peak was exhibited at 15–25°. The X-ray data of graphene@PANI nanoworm composites present crystalline peaks similar to those obtained from pure PANI, revealing that no additional crystalline order has been introduced into the composite.

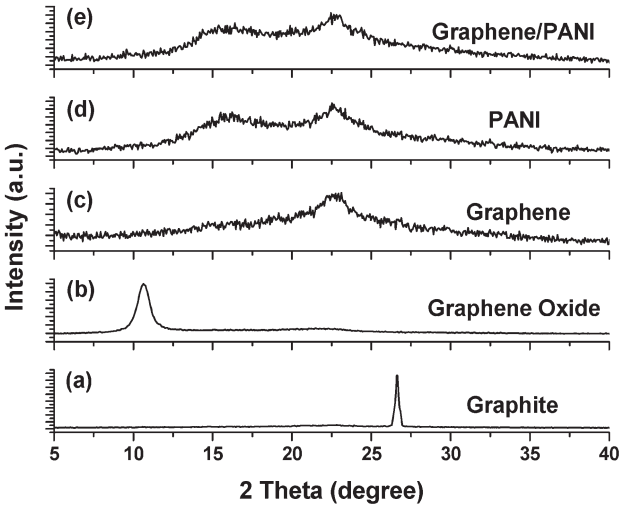

Fig. 1 XRD patterns of graphite (curve a), graphene oxide (curve b), graphene (curve c), PANI (curve d) and graphene/PANI (curve e).

Fig. 2a–c show the SEM images of the as-synthesized PANI nanoworms at low, medium and high magnifications, respectively. It also clearly demonstrates the formation of worm-like PANI nanostructure materials with a high yield. In addition, the intensive thorn-like convex morphology was generated on the surface of PANI, and the nanoworms are interconnected with each other, forming a highly porous surface morphology. Careful examination reveals that these worm-like agglomerates are 1–2 μm in length and have a diameter of about 0.2–0.3 μm, and almost all of them possess the same morphology. Fig. 2d indicates that the original graphene material consists of randomly aggregated, thin, crumpled nanosheets closely restacking with one another and forming a disordered solid. Fig. 2e–f show the representative SEM images for the graphene@PANI nanoworm composites at different magnifications. From the SEM observations, no significant change in the morphology was observed in comparison to the PANI nanoworms. Further observation indicates that the surface of PANI nanoworms are distinctly enwrapped with gauze-like graphene nanosheets and assembled into the hierarchical nanoarchitectures. To provide further insights into the morphology and structure of the resulting PANI nanoworms and graphene@PANI nanoworms, TEM investigations were carried out. Fig. 3a and b show a portion of the PANI nanoworm structure, it better illustrates that PANI really displays the worm-like structure, and its surface formation contains many thorns, which greatly increase the surface area of the PANI. Fig. 3c and d show a portion of the graphene@PANI nanoworm hierarchical nanostructure. Across the core/shell structure, it is clearly observed that the

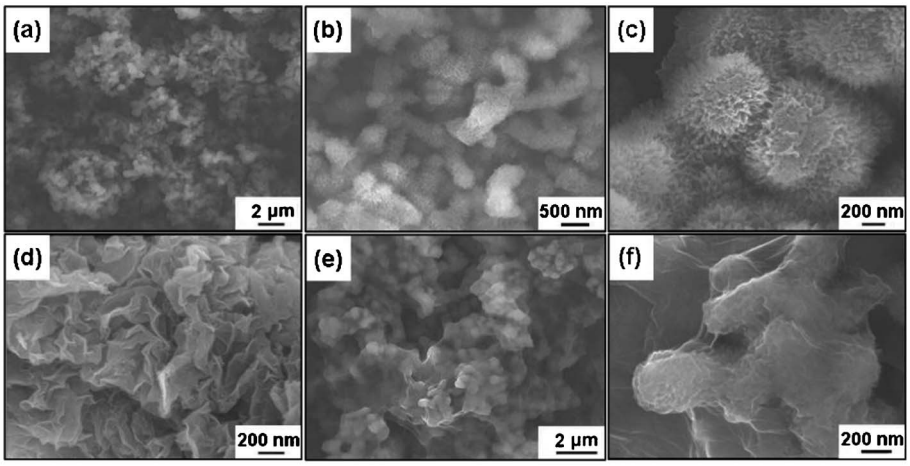

Fig. 2 (a–c) SEM images of PANI nanoworms at different magnifications; (d) SEM image of the as-prepared graphene; (e, f) low-magnification and enlarged SEM images of the graphene@PANI nanoworms.

ultrathin graphene is located around the PANI nanoworm surface. In addition, the specific surface area of PANI and graphene@PANI nanoworm were determined by nitrogen adsorption–desorption measurement at 77.35 K (as shown in Fig. S3a, ESI†). The specific surface area of the PANI and graphene@PANI nanoworms were calculated by the Brunauer–Emmett–Teller (BET) method and the values are 40.5 $m^2\ g^{-1}$ and 26.12 $m^2\ g^{-1}$, respectively. This is attributed to the fact that the PANI nanoworms have a thorn-like structure growing radially from the fiber core, and the remarkable decrease of specific surface area for the graphene@PANI nanoworms is partially attributed to the disappearance of micropores during the process of surface coating.[34] Barrett–Joyner–Halenda (BJH) calculations for the pore size distribution, derived from desorption data, reveal a narrow distribution for the thorn-like nanostructures centered at less than 50 nm (Fig. S3b, ESI†).

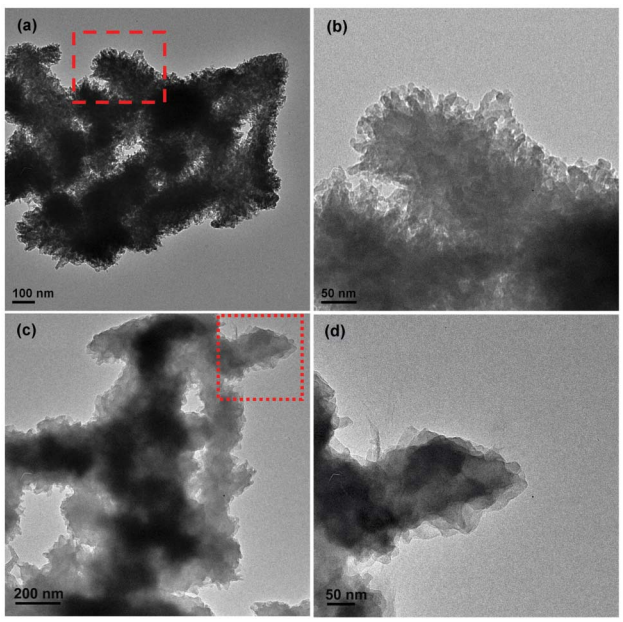

Fig. 3 (a) Low-magnification TEM image of PANI nanoworms; (b) enlarged image of the area marked by a rectangle in panel a; (c) low-magnification TEM image of graphene@PANI nanoworms composite; (d) enlarged image of the area marked by a rectangle in panel c.

The self-assembly of graphene@PANI nanoworms is illustrated in Fig. 4. It can be seen that the whole process involves three steps. Firstly, a lot of aniline monomer molecules were connected one by one *via* H-bonding leading to the formation of PANI macromolecular chain in the presence of a strong acid dopant. These acids form micelles upon which aniline is polymerized and doped. Here the –NH group in the polymer, which interacts with the surfactant molecules, provides chemical flexibility to the system.[35] In order to comprehend more clearly the formation process of PANI molecular chain in the images that follow, we also provide the polymerization mechanism as shown in Fig. S1, ESI.† Afterwards, the initial chains grow and more PANI chains are formed and gathered, then the worm-like PANI nanostructure was obtained. Finally, PANI nanoworms and GO reacted with hydrazine hydrate in solution to produce hierarchical graphene@PANI nanoworm composites.

Raman spectroscopy provides a powerful tool for characterizing the microstructure of nanosized materials. Fig. 5 demonstrates the Raman spectra of pure PANI nanoworms, graphene and graphene@PANI nanoworm composites. As shown in Fig. 5a, the out-of-plane C–H wag, out-of-plane C–N–C torsion, imine deformation, in-plane C–H bending, in-plane ring deformation, $C\text{–}N^{\cdot+}$ stretching, C=N stretching of quinoid, and C–C stretching of benzoid are situated at 412, 516, 769, 1164, 1210, 1316, 1494, and 1593 cm^{-1}, respectively.[36–38] For graphene, the Raman spectrum (Fig. 5b) displays two prominent peaks at 1339 and 1586 cm^{-1}, corresponding to the well-documented D and G bands,

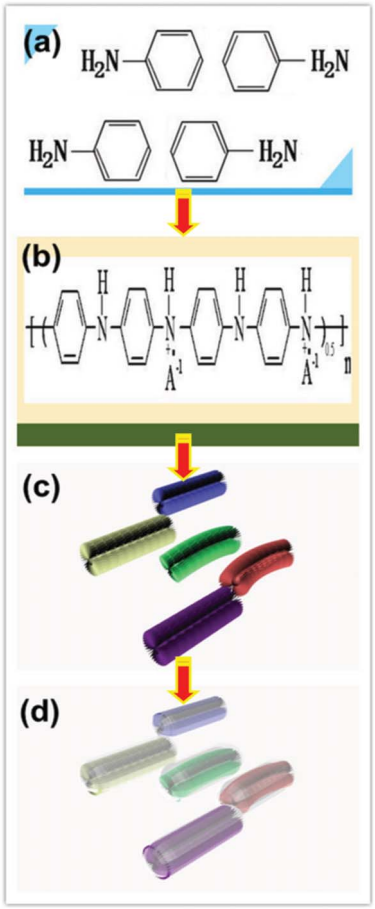

Fig. 4 Schematic representation for the formation processes of graphene@PANI nanoworms; (a) aniline; (b) PANI; (c) PANI nanoworms; (d) graphene@PANI nanoworms.

respectively. The D band corresponds to the conversion of a sp^2-hybridized carbon to a sp^3-hybridized carbon, and the G band represents the vibration of sp^2-hybridized carbon.[39] In addition, the intensity of the D band and the G band are highly similar for graphene, explaining that the graphene has a low defect content.[40] Similarly, for the Raman spectrum of graphene@PANI nanoworm composites, the Raman signals for PANI cannot be clearly observed in the composite because the PANI nanoworms have been enveloped by the graphene sheets. This demonstrates that the graphene@PANI nanoworm assemblies are well wrapped in the layer of graphene sheets.

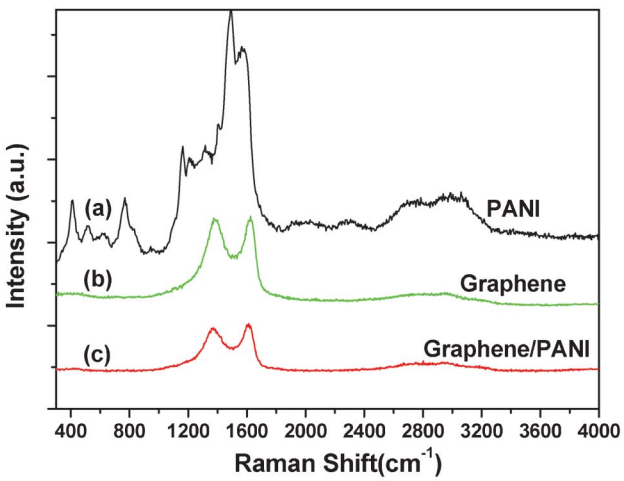

Fig. 5 Raman spectra of PANI (curve a), graphene (curve b) and graphene@PANI nanoworms (curve c).

To estimate the surface electronic state and the composition of the final products, we carried out an XPS study (Fig. 6). The survey scan spectrum of the graphene@PANI nanoworm composites in Fig. 6a shows that there are only four elements (C, N, O, and S) existing on the surface of the sample with no evidence of impurities. The presence of a sulfide peak indicates that pure PANI nanoworms and PANI in graphene@PANI nanoworm composites were both completely doped with SO_4^{2-}.[41] The high resolution C 1s spectrum of graphene@PANI nanoworm composites is shown in Fig. 6b. The deconvolution peaks of the C 1s spectrum are resolved into five components, centered at 284.8, 285.4, 286.5, 288.3 and 291.1 eV.[42] The lowest binding energy feature (284.8 eV) is due to the nonoxygenated carbon (C–C) group in the aromatic ring. The second peak is due to C–N bonds (285.4 eV). The feature at 286.5 eV can be attributed to C–O. The C 1s of the C=O peak increased to 288.3 eV, indicating that the COOH groups of graphene were wrapped upon the surface of PANI nanoworms. In addition, the π–π^* shakeup satellite peak around 291.1 eV, a characteristic of aromatic or conjugated systems, appeared after reaction, which means that conjugation in the composites increased.[43] Fig. 6c presents the XPS spectrum of the N 1s core level of graphene@PANI nanoworm composites, which indicates that it exists in three different electronic states: the benzenoid amine (–NH–) with binding energy centered at 399.6 eV, the quinoid amine (–N=) with binding energy at 398.8 eV, and the nitrogen cationic radical ($N^{+\cdot}$) with binding energy at 401.2 eV.[44] The XPS peak of the O 1s of graphene@PANI nanoworms (Fig. 6d) is composed of two Gaussian peaks with the binding energy of C–OH/C–O–C at 533.6 eV and C=O at 531.5 eV. The downshift of C=O peak reveals the increased outer electron cloud density of oxygen atoms after doping.[45] In addition, the C 1s and O 1s XPS spectra of the graphene are shown in Fig. S2, ESI.†

To demonstrate the advantage of its unique structure and further explore the potential applications of supercapacitor devices, electrochemical tests were carried out in a three-electrode configuration with a Pt plate counter electrode and an Ag/AgCl reference electrode in 1 M H_2SO_4 aqueous electrolyte solution. Fig. 7a shows the CVs of the graphene@PANI nanoworm electrode at scan rates of 10–200 mV s^{-1} in the potential range from −0.1 to 0.9 V. Three couples of redox peaks are observed and the CV curve with considerably high current and capacity exhibits an approximate rectangular shape, indicating that the supercapacitor has large double-layer capacitance. For comparison, the CV of the pristine Ti sheet, PANI, and graphene at 200 mV s^{-1} are

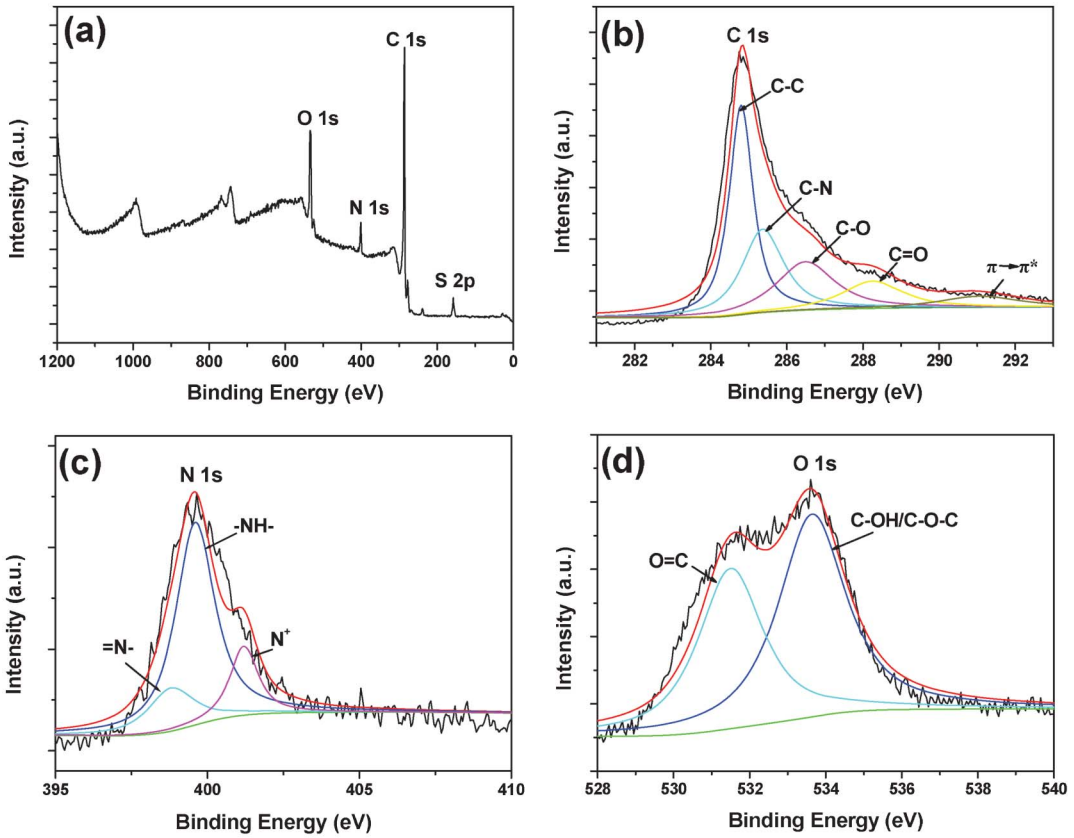

Fig. 6 (a) Survey XPS spectra of graphene@PANI nanoworms; (b),(c) and (d) XPS data of the C 1s, N 1s and O 1s regions of the graphene/PANI nanoworms, respectively.

also shown in Fig. 7b. It is noted that the current density of the graphene@PANI nanoworms at the same scan rate is higher than other electrode materials. The significant increase of the CV integrated area suggests that the graphene@PANI electrode has a much higher specific capacitance, as will be discussed. The graphene shows only one pair of redox peaks due to the transition between quinone/hydroquinone groups, which is typical for carbon materials.[46] However, compared with the graphene electrode, two couples of redox peaks appear in the CV curve of the graphene@PANI electrode, which are attributed to the transitions between a semiconducting state (leucoemeraldine form) and a conducting state (polaronic emeraldine form) and the Faradaic transformation of emeraldine–pernigraniline, respectively.[7,47] Therefore, the excellent electrochemical capability of the graphene@PANI electrode may be attributed to its unique composite microstructures, which can contribute to the rapid intercalation of cations (H^+) in the electrode during reduction and deintercalation upon oxidation. The graphene@PANI nanoworms were also characterized using galvanostatic charge–discharge measurements, as shown in Fig. 7c. It can be seen that all the curves are highly linear and symmetrical at various current densities from 0.6 to 3.0 A g^{-1}. This implies that the electrode has excellent electrochemical reversibility and charge–discharge properties. Furthermore, the specific capacitance can be calculated according to the above-mentioned equations from the discharge curves. The rate performance of graphene@PANI nanoworm composites were evaluated by charge–discharge at different current densities and compared with that of PANI nanoworm composites (Fig. 7d). The specific capacitance of the graphene@PANI nanoworms at 0.4, 0.6, 0.8, 1.0, 2.0, and 3.0 A g^{-1} is 601.4, 433.5, 353, 309.8, 234.2, and 196 F g^{-1}, respectively.

The cycle performance of the pure PANI and graphene@PANI nanoworms electrodes was examined at 400 mV s^{-1} and the results are shown in Fig. 8a. It was found that the specific capacitance of pure PANI nanoworms is about 301.4 F g^{-1} at first cycle, and the pure PANI nanoworms electrode capacitance retention is about 72.4% of initial value after 1000 cycles; the morphological and electrochemical property changes of pure PANI induced by charge–discharge cycling were reduced. However, under the same conditions, the capacitance of the graphene@PANI nanoworm composites decreased about 21.3% (from 601.4 F g^{-1} to 472.1 F g^{-1}). The improved electrochemical stability of the graphene@PANI nanoworm composites can be explained as follows. In the composite, PANI nanoworms act as the framework for sustaining graphene, preventing the nanoworms from severely swelling and shrinking during the cycle process. The graphene@PANI nanoworm electrode exhibits a good long-

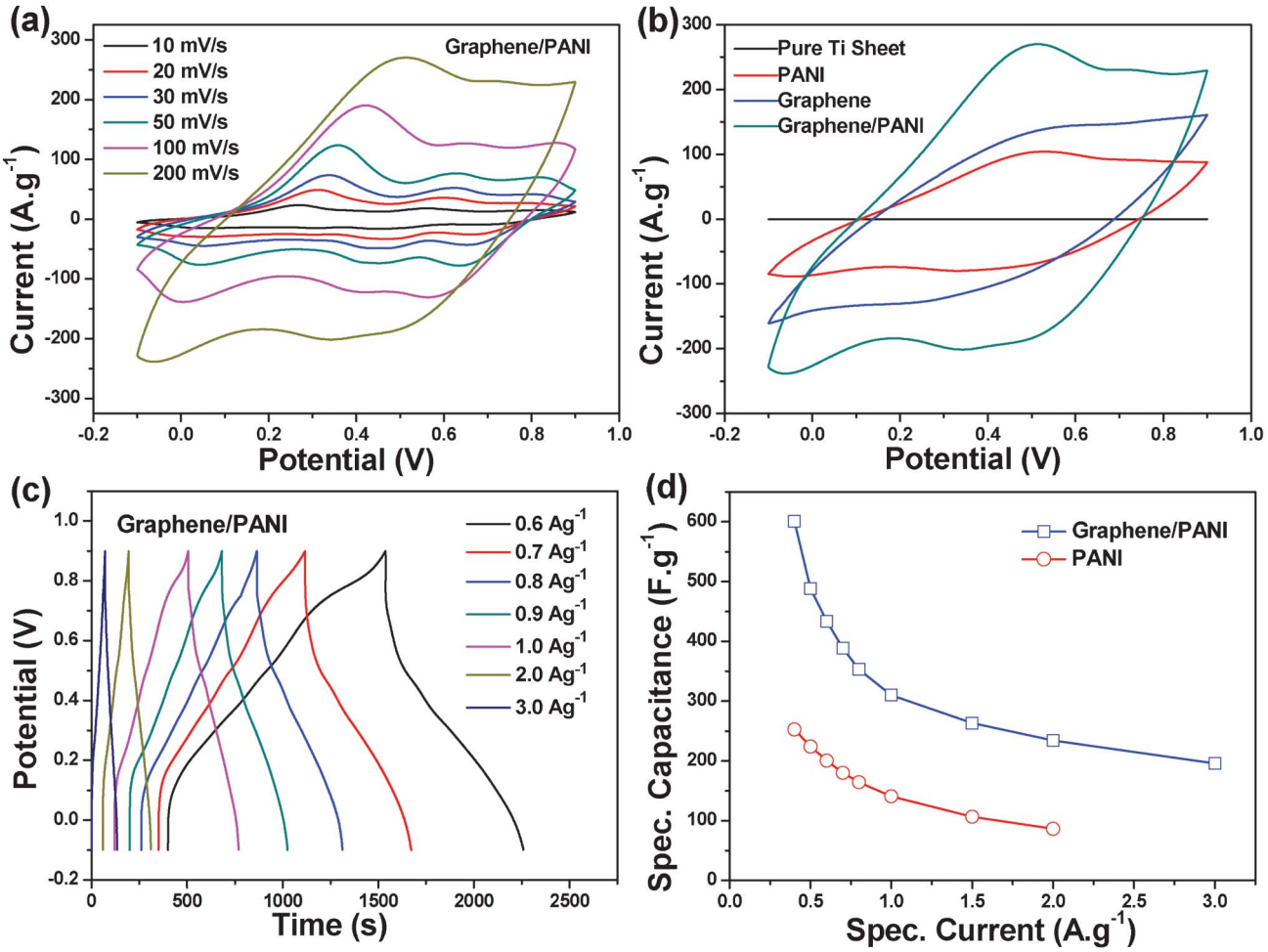

Fig. 7 (a) Cyclic voltammograms of graphene@PANI nanoworms at different scan rates; (b) cyclic voltammograms of the different electrode materials at 200 mVs^{-1}; (c) charge–discharge curves of graphene@PANI nanoworms at various current densities; (d) current density dependence of the specific capacitance of graphene@PANI nanoworms (blue curve) and PANI nanoworms (red curve).

term electrochemical stability, which is evident from the very stable charge–discharge curves for the last 21 cycles (Fig. 8b). The results indicated that the charge curves are still very symmetric to their corresponding discharge counterparts, showing no significant structural change of the graphene@PANI nanoworm electrode during the charge–discharge processes and good cycling stability. Furthermore, for a better understanding of the synergistic effect in this electrode design, the cycling performance of the graphene@PANI nanoworm composites at progressively increased current density was recorded in Fig. 8c. During the first 50 cycles with a charge–discharge density of 0.4 A g^{-1}, the hybrid structure shows a cycle stability performance of 601.4 F g^{-1}. In the following 250 cycles, as the charge/discharge rate changes successively, the hybrid structure always demonstrates stable capacitance even suffering from a sudden change of the current delivery. The CV curves before the charge–discharge test and after 1000 cycles are shown in the inset of Fig. 8a. Two couples of redox peaks could be observed and the CV curve with considerably high redox current and capacity exhibits a rectangular shape, indicating both electric double layer capacitor (EDLC) and pseudocapacitance performance of the electrode. After 1000 cycles, the redox peaks become weak and nearly disappear, this results from the reduced pseudocapacitance of PANI.

EIS analysis has been recognized as one of the principal methods examining the fundamental behavior of electrode materials for supercapacitors. To further understand the advantage of this electrode material device, impedance spectra of the graphene@PANI nanoworm composites were measured at open circuit potential with an alternating current (AC) voltage amplitude of 5 mV in the frequency range from 0.01 Hz to 100 KHz. Fig. 8d shows that the resulting Nyquist plot exhibits two distinct parts including an arc in the high frequency region and a sloped line in the low frequency region, further demonstrating the long-term electrochemical stability of this electrode material. At low frequency, the composite electrodes exhibit a more vertical line than pure PANI, showing a better capacitor behavior. At higher frequency, the impedance plot has a relatively small radius, which shows lower

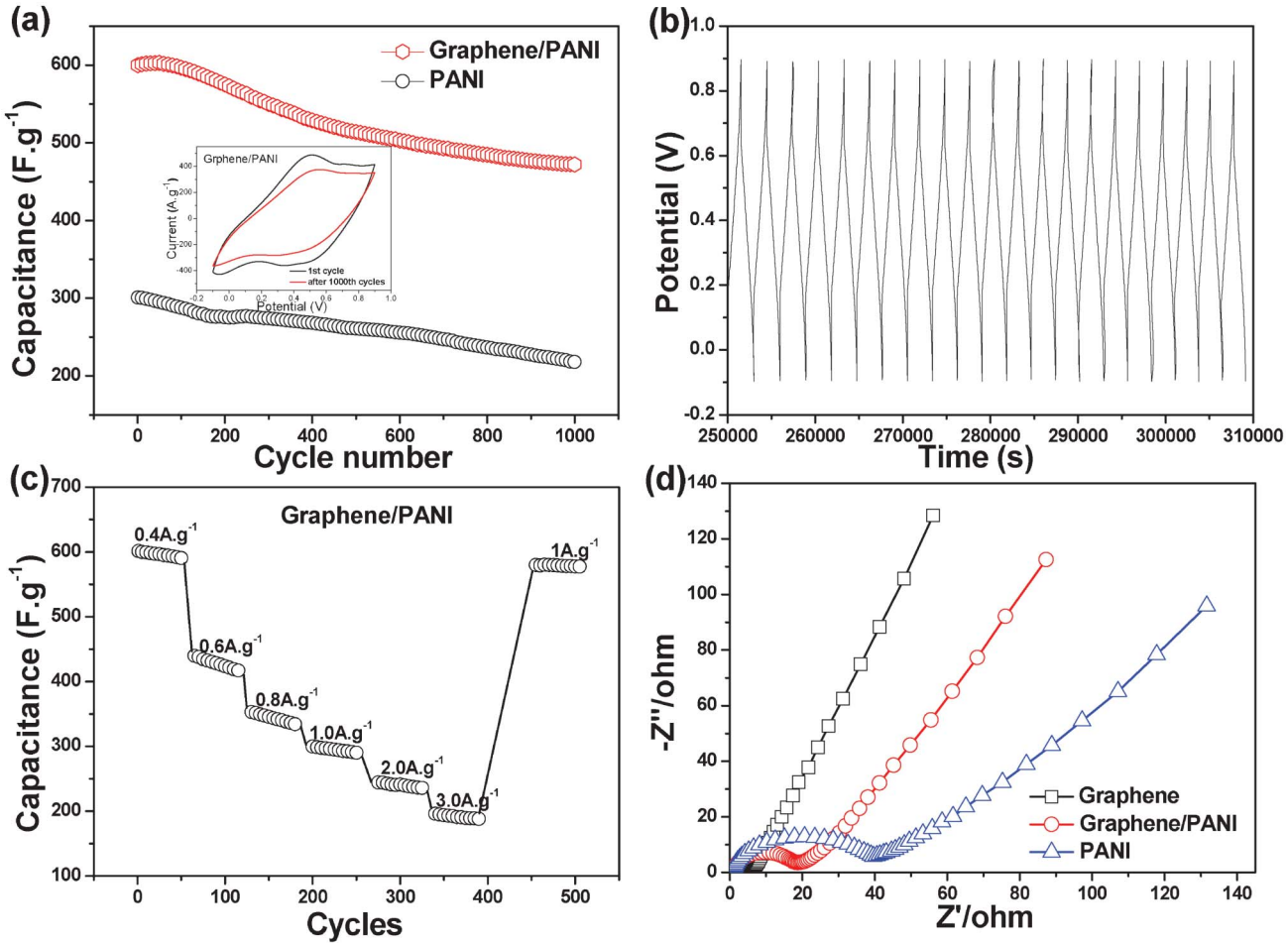

Fig. 8 (a) Cycling performance of graphene@PANI nanoworms and PANI nanoworms (inset: comparison of the CV curves before charge-discharge test and after 50 cycles for charge–discharge test at 200 mVs^{-1}); (b) the charge–discharge curves of the last 21 cycles for the graphene@PANI nanoworms; (c) cycling stability of the graphene@PANI nanoworms at progressively varying current densities; (d) Nyquist plots of graphene, graphene@PANI nanoworm, and PANI nanoworm electrodes.

resistance.[45] From the point intersecting with the real axis in the range of high frequency, the internal resistance of graphene and graphene@PANI nanoworms are much lower than that of PANI. Compared with the PANI electrode, the decreased internal resistance of the graphene@PANI nanoworm composite may be attributed to the doping process and π–π stacking between graphene and PANI nanoworms,[48] allowing the structure to facilitate the efficient access of electrolyte ions to the electrode surface and shorten the ion diffusion path.[49]

4 Conclusion

In summary, we have demonstrated an efficient strategy toward the synthesis of hierarchical graphene@PANI nanoworm composites. The results show that the integration of graphene and the worm-like PANI enables such hybrids to possess excellent electrochemical properties that are very useful and critical use as electrode materials in supercapacitors. The introduction of graphene into the nanocomposite electrodes is favorable for increasing their electrical conductivity and flexibility. On the other hand, graphene also plays a role of protection and support for the morphology structure of PANI. Meanwhile, the novel hierarchical nanostructures could effectively reduce the kinetic difficulties for both charge transfer and ion transport throughout the electrode. The maximum specific capacitance is 601.4 F g^{-1} (based on graphene@PANI nanoworm composites) at 0.4 A g^{-1} compared to 301.1 F g^{-1} for pure PANI nanoworms. The integration of hierarchical PANI nanoworms and the conducting graphene may induce a positive synergistic effect and contribute to the enhanced electrochemical performances. These intriguing features make it quite a suitable and promising electrode material for supercapacitors.

Acknowledgements

This work is supported by the Singapore National Research Foundation under NRF RF Award No. NRF-RF2010-07, MOE Tier 2 MOE2009-T2-1-037 and CRP Award No.: NRF-CRP4-

2008-03. The authors also acknowledge the financial support from the National Natural Science Foundation of China (No. U1204501).

References

1 J. R. Miller and P. Simon, *Science*, 2008, **321**, 651.
2 J. M. Tarascon and M. Armand, *Nature*, 2001, **414**, 359.
3 D. W. Wang, L. Feng, J. P. Zhao, W. C. Ren, Z. G. Chen, J. Tan, Z. S. Wu, L. Gentle, G. Q. Lu and H. M. Cheng, *ACS Nano*, 2009, **3**, 1745.
4 X. S. Fang, T. Y. Zhai, U. K. Gautam, L. Li, L. M. Wu, Y. Bando and D. Golberg, *Prog. Mater. Sci.*, 2011, **56**, 175.
5 Z. J. Fan, J. Yan, T. Wei, L. J. Zhi, G. Q. Ning, T. Y. Li and F. Wei, *Adv. Funct. Mater.*, 2011, **21**, 2366.
6 M. Kaempgen, C. K. Chan, J. Ma, Y. Cui and G. Gruner, *Nano Lett.*, 2009, **9**, 1872.
7 Y. G. Wang, H. Q. Li and Y. Y. Xia, *Adv. Mater.*, 2006, **18**, 2619.
8 G. R. Li, Z. P. Feng, J. H. Zhong, Z. L. Wang and Y. X. Tong, *Macromolecules*, 2010, **43**, 2178.
9 C. Niu, E. K. Sichel, R. Hoch, D. Moy and H. Tennent, *Appl. Phys. Lett.*, 1997, **70**, 1480.
10 C. C. Hu, K. H. Chang, M. C. Lin and Y. T. Wu, *Nano Lett.*, 2006, **6**, 2690.
11 K. S. Novoselov, A. K. Geim, S. V. Morozov, D. Jiang, Y. Zhang, S. V. Dubonos, I. V. Grigorieva and A. A. Firsov, *Science*, 2004, **306**, 666.
12 K. Zhang, L. L. Zhang, X. S. Zhao and J. S. Wu, *Chem. Mater.*, 2010, **22**, 1392.
13 J. S. Bunch, A. M. van der Zande, S. S. Verbridge, I. W. Frank, D. M. Tanenbaum, J. M. Parpia, H. G. Craighead and P. L. McEuen, *Science*, 2007, **315**, 490.
14 D. A. Dikin, S. Stankovich, E. J. Zimney, R. D. Piner, G. H. B. Dommett, G. Evmnenko, S. T. Nguyen and R. S. Ruoff, *Nature*, 2007, **448**, 457.
15 S. Park and R. S. Ruoff, *Nat. Nanotechnol.*, 2009, **4**, 217.
16 M. H. Liang and L. J. Zhi, *J. Mater. Chem.*, 2009, **19**, 5871.
17 J. D. Fowler, M. J. Allen, V. C. Tung, Y. Yang, R. B. Kaner and B. H. Weiller, *ACS Nano*, 2009, **3**, 301.
18 A. Vollmer, X. L. Feng, X. Wang, L. J. Zhi, K. Mullen, N. Koch and J. P. Rabe, *Appl. Phys. A: Mater. Sci. Process.*, 2009, **94**, 1.
19 R. Ruoff, *Nat. Nanotechnol.*, 2008, **3**, 10.
20 J. L. Xia, F. Chen, J. H. Li and N. J. Tao, *Nat. Nanotechnol.*, 2009, **4**, 505.
21 S. R. C. Vivekchand, C. S. Rout, K. S. Subrahmanyam, A. Govindara and C. N. R. Rao, *J. Chem. Sci.*, 2008, **120**, 9.
22 Y. Cao and T. E. Mallouk, *Chem. Mater.*, 2008, **20**, 5260.
23 G. A. Snook and G. Z. Chen, *J. Electroanal. Chem.*, 2008, **612**, 140.
24 K. C. Mai, M. Q. Zhang, H. M. Zeng and S. C. Qi, *J. Appl. Polym. Sci.*, 1994, **51**, 57.
25 J. P. Ferraris, M. M. Eissa, I. D. Brotherston and D. C. Loveday, *Chem. Mater.*, 1998, **10**, 3528.
26 S. Palaniappan and S. L. Devi, *J. Appl. Polym. Sci.*, 2008, **107**, 1887.
27 K. R. Prasad and N. Munichandraiah, *J. Power Sources*, 2002, **112**, 443.
28 Q. Wu, Y. Xu, Z. Yao, A. Liu and G. Shi, *ACS Nano*, 2010, **4**, 1963.
29 H. Wang, Q. Hao, X. Yang, L. Lu and X. Wang, *Nanoscale*, 2010, **2**, 2164.
30 J. C. Chiang and A. G. MacDiarmid, *Synth. Met.*, 1986, **13**, 193.
31 W. S. Hummers and R. E. Offeman, *J. Am. Chem. Soc.*, 1958, **80**, 1339.
32 W. W. Zhou, J. X. Zhu, C. W. Cheng, J. P. Liu, H. P. Yang, C. X. Cong, C. Guan, X. T. Jia, H. J. Fan, Q. Y. Yan, C. M. Li and T. Yu, *Energy Environ. Sci.*, 2011, **4**, 4954.
33 Y. S. Luo, J. Jiang, W. W. Zhou, H. P. Yang, J. S. Luo, X. Y. Qi, H. Zhang and T. Yu, *J. Mater. Chem.*, 2012, **22**, 8634.
34 J. Zhang and X. S. Zhao, *J. Phys. Chem. C*, 2012, **116**, 5420.
35 R. P. Pant, S. K. Dhawan, A. N. D. Kataria and D. K. Suri, *Ind. J. Eng. Mater. Sci.*, 2004, **11**, 267.
36 R. Ganesan, S. Shanmugam and A. Gedanken, *Synth. Met.*, 2008, **158**, 848.
37 M. G. Markovic, J. G. Matisons, R. Cervini, G. P. Simon and P. M. Fredericks, *Chem. Mater.*, 2006, **18**, 6258.
38 Z. Wei, M. Wan, T. Lin and L. Dai, *Adv. Mater.*, 2003, **15**, 136.
39 K. N. Kudin, B. Ozbas, H. C. Schniepp, R. K. Prudhomme, I. A. Aksay and R. Car, *Nano Lett.*, 2008, **8**, 36.
40 X. L. Li, X. R. Wang, L. Zhang, S. W. Lee and H. J. Dai, *Science*, 2008, **319**, 1229.
41 X. M. Feng, R. M. Li, Y. W. Ma, R. F. Chen, N. E. Shi, Q. L. Fan and W. Huang, *Adv. Funct. Mater.*, 2011, **21**, 2989.
42 Y. S. Luo, J. S. Luo, J. Jiang, W. W. Zhou, H. P. Yang, X. Y. Qi, H. Zhang, H. J. Fan, D. Y. W. Yu, C. M. Li and T. Yu, *Energy Environ. Sci.*, 2012, **5**, 6559.
43 X. B. Fan, W. C. Peng, Y. Li, X. Y. Li, S. L. Wang, G. L. Zhang and F. B. Zhang, *Adv. Mater.*, 2008, **20**, 4490.
44 M. G. Han, S. K. Cho, S. G. Oh and S. S. Im, *Synth. Met.*, 2002, **126**, 53.
45 H. L. Wang, Q. L. Hao, X. J. Yang, L. D. Lu and X. Wang, *ACS Appl. Mater. Interfaces*, 2010, **2**, 821.
46 Y. R. Nian and H. S. Teng, *J. Electrochem. Soc.*, 2002, **149**, A1008.
47 X. B. Yan, J. T. Chen, J. Yang, Q. J. Xue and P. Miele, *ACS Appl. Mater. Interfaces*, 2010, **2**, 2521.
48 Y. W. Lin and T. M. Wu, *Compos. Sci. Technol.*, 2009, **69**, 2559.
49 J. Li, H. Q. Xie, Y. Li, J. Liu and Z. X. Li, *J. Power Sources*, 2011, **196**, 10775.